International Journal of Heat and Mass Transfer 52 (2009) 5932–5939

Contents lists available at ScienceDirect

International Journal of Heat and Mass Transfer

journal homepage: www.elsevier.com/locate/ijhmt

Magnetohydrodynamic simulations using radial basis functions

Marcelo J. Colaço [a,*], George S. Dulikravich [b,1], Helcio R.B. Orlande [a]

[a] Federal University of Rio de Janeiro, Department of Mechanical Engineering, Cid. Universitaria, Cx. Postal 68503, Rio de Janeiro, RJ 21941-972, Brazil
[b] Florida International University, Department of Mechanical and Materials Engineering, 10555 West Flagler St., EC 3462, Miami, FL 33174, USA

ARTICLE INFO

Article history:
Received 16 February 2009
Received in revised form 16 August 2009
Available online 16 September 2009

Keywords:
Radial basis functions
Magnetohydrodynamic
Meshless methods

ABSTRACT

To overcome the computational mesh quality difficulties, mesh-free methods have been developed. One of the most popular mesh-free kernel approximation techniques is radial basis functions (RBFs). Initially, RBFs were developed for multivariate data and function interpolation. It is well-known that a good interpolation scheme also has great potential for solving partial differential equations. In the present study, the RBFs are used to interpolate stream-function and temperature in a two-dimensional thermal buoyancy flow acted upon by an externally applied steady magnetic field. Use of mesh-free methods promises to significantly reduce the computing time, especially for the complex classes of problems such as magnetohydrodynamics.

1. Introduction

Radial basis functions are essential ingredients of the techniques generally known as "meshless methods". In one way or another all meshless techniques require some sort of radial function to measure the influence of a given location on another part of the domain. The use of radial basis functions (RBF) followed by collocation, a technique first proposed by Kansa [1], after the work of Hardy [2] on multivariate approximation, is now becoming an established approach and various applications to problems of structures and fluids have been made in recent years. See, for example, Leitão [3,4].

Kansa's method (or asymmetric collocation) starts by building an approximation to the field of interest (normally displacement components) from the superposition of radial basis functions (globally or compactly supported) conveniently placed at points in the domain (and, or, at the boundary).

The unknowns (which are the coefficients of each RBF) are obtained from the (approximate) enforcement of the boundary conditions as well as the governing equations by means of collocation. Usually, this approximation only considers regular radial basis functions, such as the globally supported multiquadrics or the compactly supported Wendland [5] functions.

Radial basis functions (RBFs) may be classified into two main groups:

1. the globally supported ones namely the multiquadric (MQ, $\sqrt{(x-x_j)^2+c_j^2}$, where c_j is a shape parameter), the inverse multiquadric, thin plate splines, Gaussians, etc;
2. the compactly supported ones such as the Wendland [5] family (for example, $(1-r)_+^n + p(r)$ where $p(r)$ is a polynomial and $(1-r)_+^n$ is 0 for r greater than the support).

In a very brief manner, interpolation with RBFs may take the form:

$$s(x_i) = f(x_i) = \sum_{j=1}^{N} \alpha_j \phi(|x_i - x_j|) + \sum_{k=1}^{\hat{N}} \beta_k p_k(x_i) \tag{1}$$

where $f(x_i)$ is known for a series of points x_i and $p_k(x_i)$ is one of the $\hat{N}$ terms of a given basis of polynomials [6]. This approximation is solved for the α_j unknowns from the system of N linear equations, subject to the conditions (for the sake of uniqueness)

$$\sum_{j=1}^{N} \alpha_j p_k(x_j) = 0. \tag{2}$$

By using the same reasoning, it is possible to extend the interpolation concept to that of finding the approximate solution of partial differential equations. This is made by applying the corresponding differential operators to the RBFs and then to use collocation at an appropriate set of boundary and domain points. In short, the non-symmetrical collocation is the application of the domain and boundary differential operators *LI* and *LB*, respectively, to a set of N–M domain collocation points and M boundary collocation points. From this, a system of linear equations of the following type may be obtained:

* Corresponding author. Tel.: +55 21 2562 8405; fax: +55 21 2562 8383.
E-mail addresses: colaco@poli.ufrj.br (M.J. Colaço), dulikrav@fiu.edu (G.S. Dulikravich), helcio@mecanica.coppe.ufrj.br (H.R.B. Orlande).
[1] Tel.: +1 305 348 7016; fax: +1 305 348 6007.

0017-9310/$ - see front matter © 2009 Elsevier Ltd. All rights reserved.
doi:10.1016/j.ijheatmasstransfer.2009.08.009

Nomenclature

B	magnetic field
B_0	externally applied magnetic field of reference
c	shape parameter used in the radial basis functions
f	exact value of the functions at the interpolation points
g	gravity vector
Gr	Grashof number
Ha	Hartmann number
J	electric current density
L	length of the cavity
M, N	number of centers in the x and y direction, used in the RBF approximation
P	pressure
Pr	Prandtl number
r	euclidian norm between any two points
RBF	radial basis function
s	interpolated functions
T	temperature
T_h	hot temperature
T_c	cold temperature
T_0	reference temperature
V	velocity field
x, y	coordinate axis

Greek symbols

α, β	unknown coefficients of the RBF expansion
α_T	thermal diffusivity
β_T	thermal expansion coefficient
ϕ	electric potential
η	unknown coefficients of the RBF representing the temperature and stream-function
μ_0	magnetic permeability of the vacuum
σ	electrical conductivity
υ	kinematic viscosity
ξ	base functions of the RBF representing the temperature and stream-function
ψ	stream-function

Superscript

‘	dimensionless quantities

$$LIu_h(x_i) = \sum_{j=1}^{N} \alpha_j LI\phi(|x_i - \varepsilon_j|) + \sum_{k=1}^{\hat{N}} \beta_k LIp_k(x_i)$$
$$LBu_h(x_i) = \sum_{j=1}^{N} \alpha_j LB\phi(|x_i - \varepsilon_j|) + \sum_{k=1}^{\hat{N}} \beta_k LBp_k(x_i) \quad (3.a, b)$$

subject to the conditions $\sum_{j=1}^{N} \alpha_j p_k(x_j) = 0$ where the α_j and β_k unknowns are determined from the satisfaction of the domain and boundary constraints at the collocation points.

2. Magnetohydrodynamic equations

In this paper we consider the laminar, steady and incompressible fluid flow of an electrically conducting fluid within a square cavity whose top and bottom walls are kept insulated and left and right walls are subjected to different and constant temperatures. The fluid properties are considered constants and the difference of temperature will originate a buoyancy force, which is modeled using the Boussinesq's approximation. The fluid is permeated by a constant magnetic field which will create an additional buoyancy force. The governing equations are the conservation of mass, momentum, energy, and conservation of electric charges, Ohm's law and Ampere–Maxwell's law [7,8] in a moving medium

$$\nabla \cdot \mathbf{V} = 0 \quad (4.a)$$
$$(\mathbf{V} \cdot \nabla)\mathbf{V} = -\frac{1}{\rho}\nabla P + \frac{\mathbf{J}}{\rho} \times \mathbf{B} + \nu \nabla^2 \mathbf{V} - \beta_T \mathbf{g}(T - T_0) \quad (4.b)$$
$$(\mathbf{V} \cdot \nabla)T = \alpha_T \nabla^2 T + \frac{\mathbf{J}}{\rho C_p} \cdot (-\nabla\phi + \mathbf{V} \times \mathbf{B}) \quad (4.c)$$
$$\nabla \cdot \mathbf{J} = 0 \quad (4.d)$$
$$\mathbf{J} = \sigma(-\nabla\phi + \mathbf{V} \times \mathbf{B}) \quad (4.e)$$
$$\nabla \times \frac{\mathbf{B}}{\mu_0} = \mathbf{J} \quad (4.f)$$

where μ_0 is the magnetic permeability of the vacuum. Note that the Lorentz force is represented in the momentum equations through the vector product of the electric current density and the magnetic field. Also, in the above equations, the effects of polarization and magnetization were neglected [7].

As discussed by Garandet et al. [9], the harmonic equation for the electric potential, $\nabla\phi = 0$, is valid in the fluid as in the neighboring solid media. The unique solution of the harmonic equation is $\nabla\phi = 0$ since there is always an electrically insulating boundary on which $\partial\phi/\partial n = 0$ around the enclosure. It follows that the electric field vanishes everywhere. Also, it is easy to show by substituting (4.f) into (4.d), that for a two-dimensional flow, the conservation of the electric charges is automatically satisfied, reducing the final set of equations to (4.a–c, e), with $\nabla\phi = 0$.

In the present paper, the magnetic Reynolds number $Rm = VL\sigma\mu_0$ is very small. Also, the effects of Joule heating and viscous dissipation are supposed to be very small, so we can neglect the second term on the right hand side of (4.c).

Defining the stream-function

$$u = \frac{\partial\psi}{\partial y}, \quad v = -\frac{\partial\psi}{\partial x} \quad (5.a, b)$$

and the following dimensionless quantities:

$$x' = x/L; \quad y' = y/L; \quad \psi' = \psi/\upsilon; \quad T' = (T - T_c)/(T_h - T_c) \quad (6.a\text{-}d)$$

where L is the length of the cavity and T_c and T_h are the cold the hot temperatures of the container walls, respectively, we obtain, combining (4.a) and (4.b)

$$\frac{\partial\psi'}{\partial y'}\left(\frac{\partial^3\psi'}{\partial x'\partial y'^2} + \frac{\partial^3\psi'}{\partial x'^3}\right) - \frac{\partial\psi'}{\partial x'}\left(\frac{\partial^3\psi'}{\partial y'\partial x'^2} + \frac{\partial^3\psi'}{\partial y'^3}\right) = \frac{\partial^4\psi'}{\partial x'^4} + 2\frac{\partial^4\psi'}{\partial x'^2\partial y'^2} + \frac{\partial^4\psi'}{\partial y'^4} + Ha^2\frac{\partial^2\psi'}{\partial x'^2} - Gr\frac{\partial T'}{\partial x'} \quad (7.a)$$

Also, substituting (5.a,b) into (4.c) we obtain

$$\frac{\partial\psi'}{\partial y'}\frac{\partial T'}{\partial x'} - \frac{\partial\psi'}{\partial x'}\frac{\partial T'}{\partial y'} = \frac{1}{Pr}\left(\frac{\partial^2 T'}{\partial x'^2} + \frac{\partial^2 T'}{\partial y'^2}\right) \quad (7.b)$$

where Ha, Gr and Pr are the Hartmann, Grashof and Prandtl numbers, respectively. They are defined as

$$Ha = B_0 L\sqrt{\frac{\sigma}{\mu}}; \quad Gr = \frac{g\beta_T(T_h - T_c)L^3}{\nu^2}; \quad Pr = \frac{\nu}{\alpha_T} \quad (8.a\text{-}c)$$

where B_0 is the steady externally applied magnetic field of reference.

3. Test problem formulation

The test problem analyzed here is a square cavity, where the left wall is subjected to a hot temperature and the right wall is subjected to a cold temperature. The top and bottom walls are kept thermally insulated. All four boundaries are subjected to no-slip boundary conditions and a constant magnetic field is applied in the x direction (from the left to the right wall). Notice that the bi-harmonic equation (7.a) needs two boundary conditions for each wall, which are given along the ones for Eq. (7.b)

$$\psi' = \frac{\partial \psi'}{\partial x'} = 0; \quad T' = 1 \quad \text{at } x = 0 \tag{9.a-c}$$

$$\psi' = \frac{\partial \psi'}{\partial x'} = T' = 0 \quad \text{at } x = 1 \tag{9.d-f}$$

$$\psi' = \frac{\partial \psi'}{\partial y'} = \frac{\partial T'}{\partial y'} = 0 \quad \text{at } y = 0 \tag{9.g-i}$$

$$\psi' = \frac{\partial \psi'}{\partial y'} = \frac{\partial T'}{\partial y'} = 0 \quad \text{at } y = 1 \tag{9.j-l}$$

Several Hartmann numbers will be analyzed for two values of the Grashof number ($Gr = 10^4$ and $Gr = 10^6$) and the final results will be compared against Ref. [10] where the authors used the control volume method on a uniform grid of 40×40 grid cells. The Prandtl number was equal to 0.71 in all test cases.

4. Radial basis function approximation

Classical numerical methods, such as the finite volume method and the finite difference method, need to use some kind of pressure–velocity coupling scheme (for example, SIMPLEC Scheme [11]) in order to obtain velocity fields in the momentum equation (4.b) that satisfies the mass conservation equation (4.a). On the other hand, in such methods, the use of the bi-harmonic equation (7.a), which eliminates the pressure gradient, brings several problems of truncation error in the derivative approximations of the 4th order derivatives. Also, the convective terms are usually treated by some sort of hybrid or upwind method, such as the WUDS [12] and the UTOPIA [13] algorithms.

In this paper, we use a RBF formulation to solve the Eqs. (7.a-b) as well as the boundary conditions (9.a-l). In the RBF formulation, the stream function and the temperature are written as

$$\psi'(x', y') = \sum_{i=1}^{M} \eta_i \xi(\mathbf{r}_i) \tag{10.a}$$

$$T'(x', y') = \sum_{j=1}^{N} \lambda_j \xi(\mathbf{r}_j) \tag{10.b}$$

where the RBFs ξ are the same for the two expansions, but the parameters η and λ are different for each one. In Eqs. (10.a, b), M and N are the number of centers used in the two RBF approximations.

Substituting Eqs. (10.a,b) into Eqs. (7.a,b) we can obtain

$$\begin{aligned}
&\sum_{i=1}^{M}\left[\eta_i \frac{\partial \xi(\mathbf{r}_i)}{\partial y'}\right]\left\{\sum_{i=1}^{M}\left[\eta_i \frac{\partial^3 \xi(\mathbf{r}_i)}{\partial x' \partial y'^2}\right] + \sum_{i=1}^{M}\left[\eta_i \frac{\partial^3 \xi(\mathbf{r}_i)}{\partial x'^3}\right]\right\} \\
&\quad - \sum_{i=1}^{M}\left[\eta_i \frac{\partial \xi(\mathbf{r}_i)}{\partial x'}\right]\left\{\sum_{i=1}^{M}\left[\eta_i \frac{\partial^3 \xi(\mathbf{r}_i)}{\partial y' \partial x'^2}\right] + \sum_{i=1}^{M}\left[\eta_i \frac{\partial^3 \xi(\mathbf{r}_i)}{\partial y'^3}\right]\right\} \\
&\quad = \sum_{i=1}^{M}\left[\eta_i \frac{\partial^4 \xi(\mathbf{r}_i)}{\partial x'^4}\right] + 2\sum_{i=1}^{M}\left[\eta_i \frac{\partial^4 \xi(\mathbf{r}_i)}{\partial x'^2 \partial y'^2}\right] + \sum_{i=1}^{M}\left[\eta_i \frac{\partial^4 \xi(\mathbf{r}_i)}{\partial y'^4}\right] \\
&\qquad + Ha^2 \sum_{i=1}^{M}\left[\eta_i \frac{\partial^2 \xi(\mathbf{r}_i)}{\partial x'^2}\right] - Gr \sum_{j=1}^{N}\left[\lambda_j \frac{\partial \xi(\mathbf{r}_j)}{\partial x'}\right]
\end{aligned} \tag{11}$$

$$\begin{aligned}
&\sum_{i=1}^{M}\left[\eta_i \frac{\partial \xi(\mathbf{r}_i)}{\partial y'}\right]\sum_{j=1}^{N}\left[\lambda_j \frac{\partial \xi(\mathbf{r}_j)}{\partial x'}\right] - \sum_{i=1}^{M}\left[\eta_i \frac{\partial \xi(\mathbf{r}_i)}{\partial x'}\right]\sum_{j=1}^{N}\left[\lambda_j \frac{\partial \xi(\mathbf{r}_j)}{\partial y'}\right] \\
&\quad = \frac{1}{Pr}\left\{\sum_{j=1}^{N}\left[\lambda_j \frac{\partial^2 \xi(\mathbf{r}_j)}{\partial x'^2}\right] + \sum_{j=1}^{N}\left[\lambda_j \frac{\partial^2 \xi(\mathbf{r}_j)}{\partial y'^2}\right]\right\}
\end{aligned} \tag{12}$$

Note that the boundary conditions given by Eqs. (9.a-l) should also be written in terms of the RBFs. Thus, substituting (10.a,b) into Eqs. (9.a-l) we obtain

$$\sum_{i=1}^{M} \eta_i \xi(\mathbf{r}_i) = \sum_{i=1}^{M}\left[\eta_i \frac{\partial \xi(\mathbf{r}_i)}{\partial x'}\right] = 0; \quad \sum_{j=1}^{N} \lambda_j \xi(\mathbf{r}_j) = 1 \quad \text{at } x = 0 \tag{13.a-c}$$

Table 1
Computing time (in s) for solving the MHD problem using RBFs with different number of centers and the FVM with different number of volumes for $Gr = 10^4$.

$Gr = 0^4$	CPU time (s) RBF (6×6)	CPU time (s) RBF (8×8)	CPU time (s) RBF (15×15)	CPU time (s) FVM (15×15)	CPU time (s) FVM (41×41)
$Ha = 0$	0.72	2.05	50.60	47	440
$Ha = 10$	0.66	1.70	34.03	56	560
$Ha = 15$	0.63	1.83	40.14	63	562
$Ha = 25$	0.56	1.69	42.59	69	684
$Ha = 50$	0.42	1.17	25.53	74	778

Table 2
Comparison for the average Nusselt number using RBF with a different number of centers (collocation points) and the FVM with different number of volumes for $Gr = 10^4$.

$Gr = 10^4$	Average Nusselt number										
	Ref. [10]	RBF (6×6)	Error (%)	RBF (8×8)	Error (%)	RBF (15×15)	Error (%)	FVM (15×15)	Error (%)	FVM (41×41)	Error (%)
$Ha = 0$	2.01	2.46	22.39	2.19	8.96	2.02	0.50	2.10	4.48	2.06	2.49
$Ha = 10$	1.69	2.01	18.93	1.83	8.28	1.70	0.59	1.89	11.83	1.84	8.88
$Ha = 25$	1.14	1.25	9.65	1.21	6.14	1.17	2.63	1.38	21.05	1.32	15.79
$Ha = 50$	1.00	0.89	11.00	1.02	2.00	0.97	3.00	1.10	10.00	1.06	6.00

$$\sum_{i=1}^{M}\eta_i\xi(\mathbf{r}_i)=\sum_{i=1}^{M}\left[\eta_i\frac{\partial\xi(\mathbf{r}_i)}{\partial x'}\right]=0;\quad \sum_{j=1}^{N}\lambda_j\xi(\mathbf{r}_j)=0\quad \text{at } x=1 \qquad (13.\text{d-f})$$

$$\sum_{i=1}^{M}\eta_i\xi(\mathbf{r}_i)=\sum_{i=1}^{M}\left[\eta_i\frac{\partial\xi(\mathbf{r}_i)}{\partial x'}\right]=\sum_{j=1}^{N}\left[\lambda_j\frac{\partial\xi(\mathbf{r}_j)}{\partial y'}\right]=0\quad \text{at } y=0 \qquad (13.\text{g-i})$$

$$\sum_{i=1}^{M}\eta_i\xi(\mathbf{r}_i)=\sum_{i=1}^{M}\left[\eta_i\frac{\partial\xi(\mathbf{r}_i)}{\partial x'}\right]=\sum_{j=1}^{N}\left[\lambda_j\frac{\partial\xi(\mathbf{r}_j)}{\partial y'}\right]=0\quad \text{at } y=1 \qquad (13.\text{j-l})$$

Eqs. (11)–(13) result in a non-linear system of algebraic equations which can be solved with well-established numerical procedures such as the Broyden's quasi-Newton method [14]. Several different choices are possible for the RBF function [6]. We used the multiquadric which is given as

$$\xi(\mathbf{r}_i)=\xi_i(x,y)=\sqrt{(x-x_i)^2+(y-y_i)^2+c^2} \qquad (14)$$

where c is a shape parameter used to control the smoothness of the RBF. Up to this time, there is no well-established methodology to choose this shape parameter, although some empiricism can be found in the literature [15,16]. In this work, we will use the procedure defined by [17], where c is taken as the minimum distance between two center points over the entire domain. Thus, c is increased monotonically until the residual of the solution of Eqs. (7.a,b, 9.a-l) is minimum. This procedure implies solving very costly non-linear equations several times (in this paper we limited the upper value of c to ten times its initial value), but the final result is worthy.

Note that Eqs. (11) and (12) should be written for each collocation point inside the domain. Thus, if we have L collocation points, Eqs. (11) and (12) should lead to L equations each. Also, Eqs. (13.a-l) should be written for each collocation point at the boundaries. If we

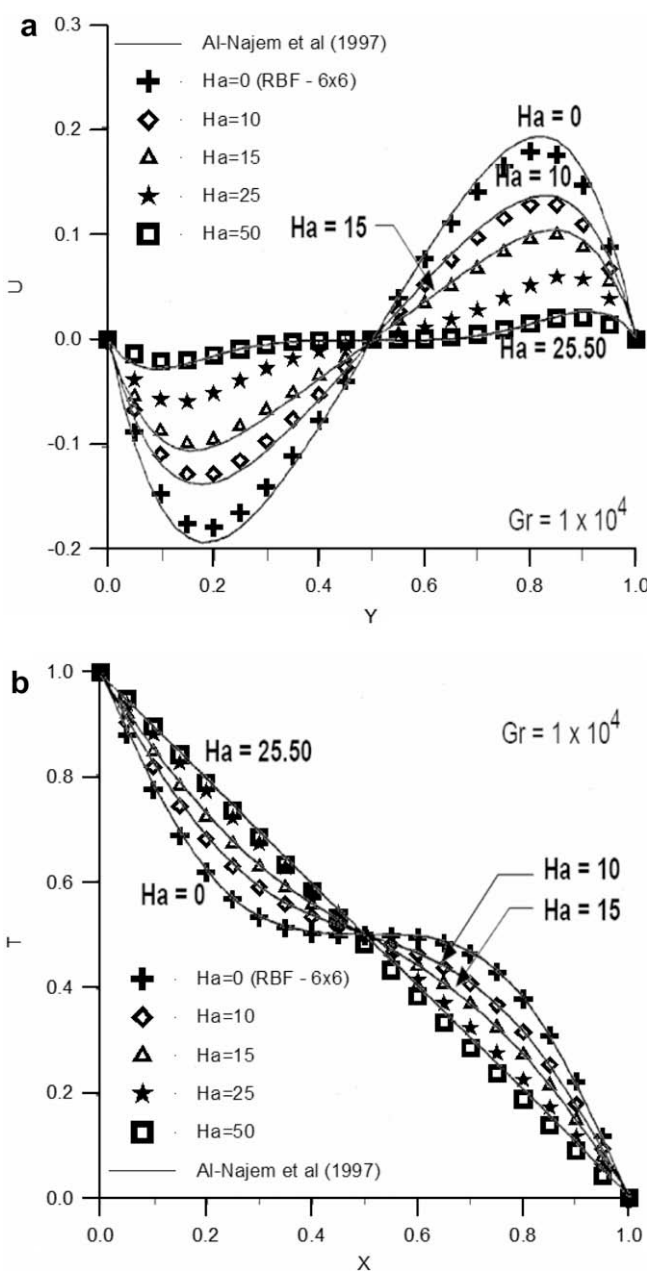

Fig. 1. Velocity and temperature profiles for 6×6 RBF centers.

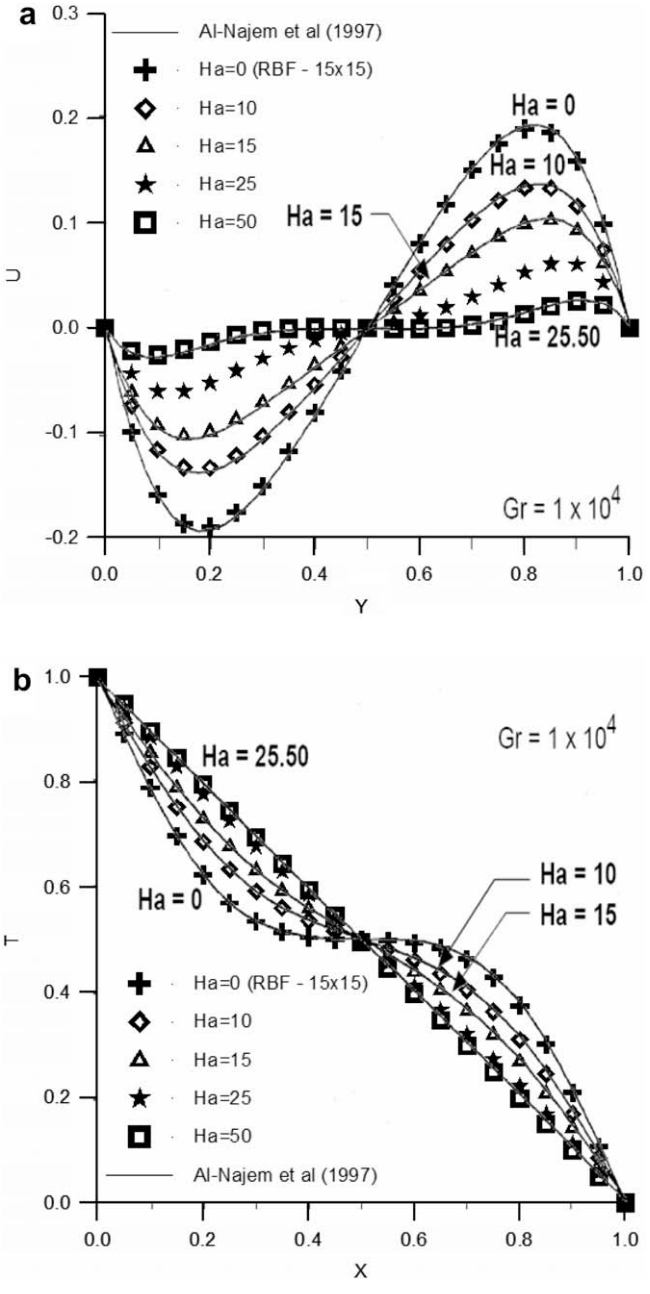

Fig. 2. Velocity and temperature profiles for 15×15 RBF centers.

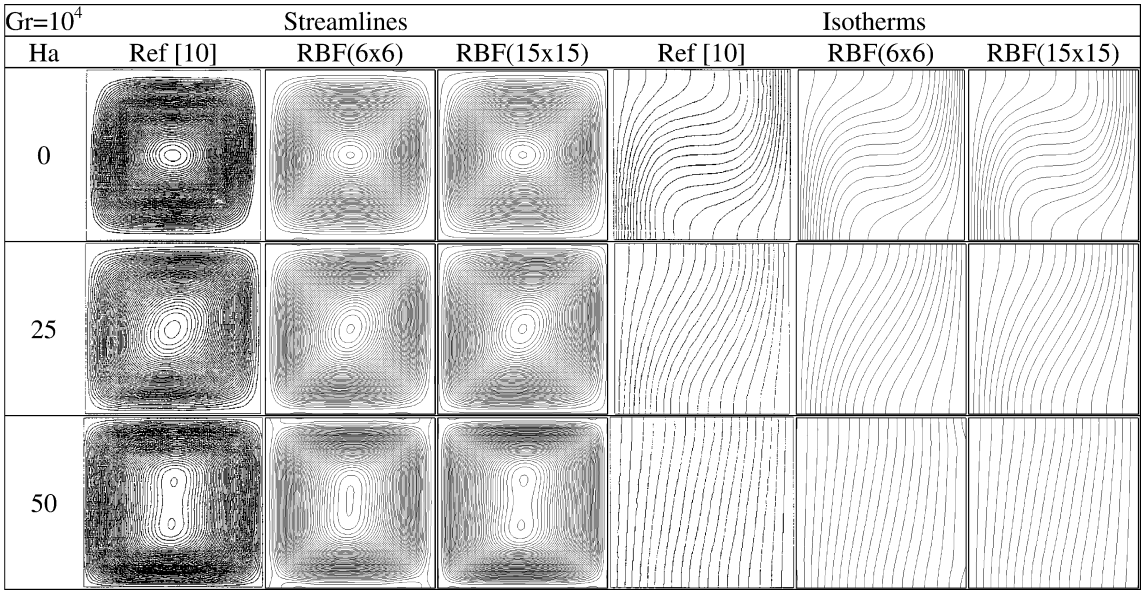

Fig. 3. Streamlines and isotherms for Ref. [10] and for RBF method.

Table 3
Computing time when solving the MHD problem using RBFs with different number of centers and the FVM with different number of volumes for $Gr = 10^6$.

$Gr = 10^6$	CPU time (s) RBF (15×15)	CPU time (s) RBF (25×25)	CPU time (s) FVM (25×25)	CPU time (s) FVM (41×41)
$Ha = 0$	134.80	1637.80	836	2593
$Ha = 10$	145.75	1288.08	919	2928
$Ha = 15$	138.00	2426.27	1014	3217
$Ha = 25$	166.58	1047.38	1058	3285
$Ha = 50$	73.09	913.36	1167	3223
$Ha = 100$	50.84	1528.84	1489	4560
$Ha = \infty$	71.52	4243.59	–	–

have P collocation points at the boundaries, the boundary conditions for the bi-harmonic equation will result in $2P$ equations and the boundary conditions for the energy equation will result in P equations, since the bi-harmonic equation is a 4th order equation and the energy equation is a 2nd order equation. It follows that, in order to have the same number of variables and equations, M should be equal to $(L + 2P)$ and N should be equal to $(L + P)$. In order to circumvent this, we adopted the same strategy used in [17], where some ghost centers are used outside of the domain for the P extra variables needed. These points are located outside of the domain, close to the boundary conditions.

5. Numerical results

In order to show how accurate the RBF-MHD formulation can be, several test cases were analyzed, and the results were compared with Ref. [10] where the authors used the control volume method [18] on a grid of 41×41 equally spaced points. They solved the vorticity conservation equation and not the bi-harmonic Eq. (7.a). Also, in their paper, the results were shown for several different inclinations of the cavity. Since the original papers [10,18] did not show the computing times required to obtain the desired solution, we also solved these problems by the finite volume method with primitive variables [8] and compared the computing time required to obtain approximately the same order of accuracy for the solutions obtained using the RBF-MHD approximation.

In this paper we considered only the case where the cavity is not tilted. Two test cases correspond to the Grashof numbers equal to $Gr = 10^4$ and $Gr = 10^6$, where several Hartman numbers were analyzed. In all test cases, $Pr = 0.71$. All test cases presented in this paper were run on an Intel Centrino Duo (T2300 @ 1.66 GHz) processor with 1 Gb of RAM memory. The code was written in FORTRAN90 and the "cpu_time" intrinsic function was used to measure the computing time.

For $Gr = 10^4$, the following Hartman numbers were analyzed: $Ha = 0$, 10, 25 and 50. Table 1 shows the computing time required to solve such problems, using several different numbers of RBF centers (collocation points) for the RBF approximation and different number of volumes for the finite volume method. Although the RBF approach does not require the use of a computing grid (the points can be randomly distributed), for the first results we used a uniformly distributed grid. It can be seen that the computing time is extremely low when solving such problems with the RBF. Although the RBF approximation with 15×15 collocation points needs approximately the same amount of computing time to solve the problem as the finite volume method with 15×15 volumes, Table 2 shows that the numerical error obtained with the RBF is an order of magnitude smaller. Also, in general, as the Hartman number increases, one can see from Table 1 that the computing time decreases for the RBF and increases for the finite volume method.

Table 2 shows the comparison for the average Nusselt number at the left and right walls computed in the present paper and in Ref. [10], for $Gr = 10^4$. This table also shows the results obtained by the finite volume method with primitive variables used in this work. From Table 2, it is clear that as we increase the number of centers in the RBF approximation, the discrepancy between these two sets of solutions becomes smaller. Ref. [10] only shows the average Nusselt number in graphics, so the ones used here for comparison were taken by measuring the graphics presented in [10] and are not necessarily error free. Keeping this in mind, the RBF-MHD formulation gives exceptionally good results, while requiring very small number of centers for its formulation. From the inspection of Table 1, most of the results were obtained in less than 30 s. A further investigation related to the choice of the shape parameter c in the RBF approximation could reduce such computing time even more. From Table 2, one can verify that it is necessary to

Table 4
Comparison of the average Nusselt numbers using RBF with a different number of centers (collocation points) and the FVM with different number of volumes for $Gr = 0^6$.

$Gr = 10^6$	Average Nusselt number								
	Ref. [10]	RBF (15×15)	Error (%)	RBF (25×25)	Error (%)	FVM (25×25)	Error (%)	FVM (41×41)	Error (%)
$Ha = 0$	8.76	10.68	21.92	9.21	5.14	8.24	5.94	7.98	8.90
$Ha = 10$	8.66	10.44	20.55	9.04	4.39	8.17	5.66	7.88	9.01
$Ha = 25$	8.04	8.92	10.95	8.32	3.48	7.81	2.86	7.39	8.08
$Ha = 100$	3.76	3.95	5.05	3.54	5.85	4.97	32.18	4.27	13.56
$Ha = \infty$	0.96	0.88	8.33	0.90	6.25	–	–	–	–

use a grid of 41×41 volumes in the finite volume method to obtain a result with approximately the same order of accuracy as the one with 15×15 centers in the RBF approximation. Thus, looking back at Table 1, one can see that the finite volume method requires at least one order of magnitude greater computing time than the RBF to obtain the same level of accuracy.

Fig. 1 shows the velocity profiles at the points located along the vertical axis and temperature along the horizontal axis of symmetry of the cavity, both for the RBF-MHD formulation with 6×6 centers and for the results presented in [10], for $Gr = 10^4$. One can see that even for this extremely low number of collocation centers, the velocity and the temperature profiles are very well captured. This becomes even more impressive when one looks at Table 1 and sees that such results were obtained in less then 1 s.

Fig. 2 shows the same results, but now using 15×15 RBF centers. One can see that the accuracy of the results improves and now the velocity profiles match the ones presented in [10], except for our results with $Ha = 25$. Actually, our results for $Ha = 50$ match results for $Ha = 25$ in [10]. This suggests that results labeled $Ha = 25$ in [10] should actually have been labeled $Ha = 50$.

Finally, Fig. 3 shows the isotherms and stream functions for $Gr = 10^4$, where it is clear that the MHD-RBF formulation gives very good results compared with the ones presented in [10], even for a very small number of centers.

The second set of test cases involved a Grashof number $Gr = 10^6$, which corresponds to conditions where the thermal buoyancy effects are two orders of magnitude stronger. Thus, the magnetic field needed to suppress such natural convection must be stronger than the one previously discussed for $Gr = 10^4$. For this higher Grashof number, the following Hartmann numbers were analyzed: $Ha = 0$, 10, 15, 25, 50, 100 and infinity. Table 3 shows the computing time required, using different number of RBF centers and also using different number of finite volumes in the finite volume method used in this work. For this set of test cases, with higher Grashof numbers, the number of required centers was greater than in the previous case with $Gr = 10^4$. Also, comparing Tables 1 and 3, one can see that, even for the same number of collocation points (15×15), the computing time for the RBF, in the case with higher Grashof number, increases by a factor greater than two for most Hartmann numbers. In general, when the Hartmann number increases, the computing time for RBF decreases. On the other hand, when the Hartmann number increases, the computing time for the finite volume method increases.

Table 4 shows the comparison for the average Nusselt number for the test cases where the Grashof number was equal to $Gr = 10^6$. Comparing Tables 2 and 4 for $Gr = 10^4$ and $Gr = 10^6$, respectively, one can see that the relative errors for the later one are higher, as expected. Such computing time could be decreased if more efficient methods to solve the non-linear system of algebraic equations were used. Also, a better strategy to choose the optimum shape factor c in the RBF approximation could lead to shorter computing times and higher accuracy. From Tables 3 and 4, one can see that, for the test case where $Gr = 10^6$, in order to have a result with approximately 5% of relative error in Nusselt number, it takes approximately 30 min of computing time when using the RBF-MHD model to solve the non-linear bi-harmonic and energy equations. Comparing the RBF-MHD method with the finite volume method, one can see that for the same order of accuracy, the RBF-MHD required 15×15 collocation centers, while the finite

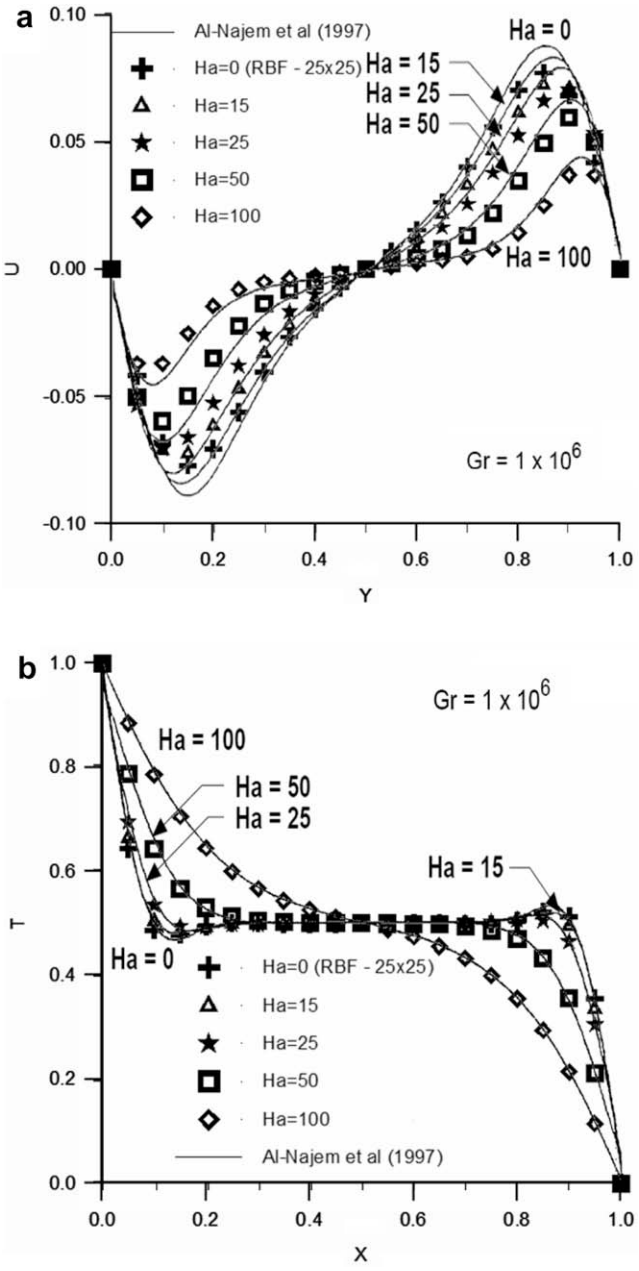

Fig. 4. Velocity and temperature profiles for 25×25 RBF centers.

volume method needed 41 × 41 finite volumes. Thus, from Table 3, the finite volume method required again a computing time that is at least one order of magnitude greater than the RBF-MHD model to obtain the same level of accuracy.

Fig. 4 shows the velocity and temperature profiles at mid-location of the cavity, both for the RBF-MHD formulation with 25 × 25 centers, and for the results presented in [10], for $Gr = 10^6$. Although the isotherms are close to the results presented in [10], the peak values of the velocities are not very well captured, showing that, for this test case 25 × 25 collocation points are not enough to solve such a strong natural convection problem. This indicates that more collocation points were needed for this test case. However, since the computing time would increase considerably, this was not conducted in this paper.

The streamlines and isotherms obtained by the RBF-MHD formulation behave in the same way as those obtained in [10], although some discrepancies were observed for the lower values of Hartmann numbers, where the mass, momentum and energy equations are more coupled.

In order to improve the accuracy of the solution, some extra results were obtained using a non-uniform distribution of centers. Four different distributions were used, where a parameter χ was used to control such non-uniformity. Fig. 5 shows the distribution of the 10 × 10 centers, for different values of the parameter χ.

Also, the possibility of using a pseudo-random distribution of collocation points was investigated. For such distribution, we used the Sobol's [19] algorithm with the constraint that the minimum distance between any two points should meet some uniformity criteria. Thus, the RBF-MHD model could be easily extended to very complex geometries, where the grid generation is an issue. Fig. 5 also shows the distribution of 10 × 10 centers, using such pseudo-random algorithm.

Table 5 shows the deviation of the average Nusselt number from the ones reported in Ref [10] for $Gr = 10^4$ and using 6 × 6 centers, for different values of parameter χ and also for a pseudo-random distribution of collocation points. From this table, the use of a non-uniform distribution of centers, with $\chi = 0.4$, reduces significantly the deviation from the results presented in [10]. As for example, the relative error for $Ha = 0$ decays from 22.39% to 5.97%. For $Ha = 10$ and 25 there is also a decay in the relative error, although for $Ha = 50$, the error increases a little. The use of a pseudo-random distribution for the collocation points also reduces significantly the error, except for the case where $Ha = 0$. In fact, for $Ha = 50$, the results obtained through this random distribution presented the lowest errors when compared to the values presented in [10]. The results when using the pseudo-random distribution of points are actually arithmetic means of results obtained on five different pseudo-randomly distributed sets of points obtained with different input parameters to Sobol's algorithm.

When more centers are used (15 × 15, instead of 6 × 6), the deviation of the average Nusselt number from the ones reported in Ref [10], for different values of parameter χ and for the pseudo-random distribution of the collocation points are presented in Table 6. For this test case, where the number of centers was already large, there was not much decrease of the relative error compared to the case where a uniform distribution of centers was used. From this Table, the best non-uniformity factor found was $\chi = 0.2$, where only the cases with $Ha = 25$ and 50 had a decrease in the relative error. Also, the pseudo-random distribution of the collocation points reduced the error to the same levels obtained with $\chi = 0.2$.

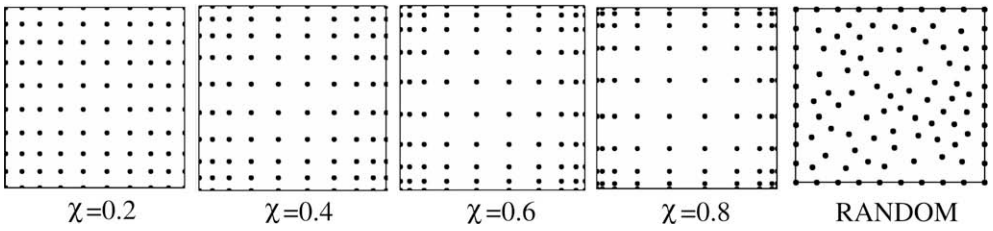

Fig. 5. Distribution of the 10 × 10 centers, for different values of the parameter χ and for a pseudo-random distribution of the collocation points.

Table 5
Influence of the non-uniformity factor χ on the relative error of the solution for 6 × 6 centers and the solution using a pseudo-random distribution of the centers.

$Gr = 10^4$	Average Nusselt number												
	Ref. [10]	RBF (6 × 6) χ=0.0	Error (%)	RBF (6×6) χ = 0.2	Error (%)	RBF (6 × 6) χ = 0.4	Error (%)	RBF (6 × 6) χ = 0.6	Error (%)	RBF (6 × 6) χ = 0.8	Error (%)	RBF (6 × 6) Random	Error (%)
$Ha = 0$	2.01	2.46	22.39	2.32	15.42	2.13	5.97	0.86	57.21	0.79	60.70	2.35	16.92
$Ha = 10$	1.69	2.01	18.93	1.93	14.20	1.76	3.57	1.39	17.75	0.79	53.25	1.90	12.43
$Ha = 25$	1.14	1.25	9.65	1.24	8.77	1.19	4.39	1.11	2.63	0.79	30.70	1.21	6.14
$Ha = 50$	1.00	0.89	11.00	0.96	4.00	0.87	13.00	0.96	4.00	0.79	21.00	1.00	0.00

Table 6
Influence of the non-uniformity factor χ on the relative error of the solution for 15 × 15 centers and the solution using a pseudo-random distribution of the centers.

$Gr = 10^4$	Average Nusselt number												
	Ref. [10]	RBF (15 × 15) χ = 0.0	Error (%)	RBF (15 × 15) χ = 0.2	Error (%)	RBF (15 × 15) χ = 0.4	Error (%)	RBF (15 × 15) χ = 0.6	Error (%)	RBF (15 × 15) χ = 0.8	Error (%)	RBF (15 × 15) Random	Error (%)
$Ha = 0$	2.01	2.02	0.50	2.02	0.50	2.00	0.50	0.86	57.21	0.79	60.70	2.00	0.50
$Ha = 10$	1.69	1.70	0.59	1.70	0.59	1.69	0.00	1.04	38.46	1.05	37.87	1.70	0.59
$Ha = 25$	1.14	1.17	2.63	1.16	1.75	1.16	1.75	1.15	0.88	0.96	15.79	1.16	1.75
$Ha = 50$	1.00	0.97	3.00	1.00	0.00	0.97	3.00	0.99	1.00	0.98	2.00	0.97	3.00

Thus, although the non-uniformity factor presented some oscillatory behavior, the pseudo-random distribution was stable and capable of producing good results. For complex geometries, where the grid generation can be difficult, such approach can be very useful.

6. Conclusions

This work used the radial basis function formulation to solve a magnetohydrodynamic problem in two dimensions in an incompressible, steady-state and laminar flow-field with constant magnetic field applied. The RBF results were compared against control volume method results reported in the literature. We also compared the computing time with a finite volume method using primitive variables. The accuracy of RBF was very good and computing time was at least an order of magnitude smaller. The use of the RBF-MHD formulation in solving complex physical problems seems to be very promising, since it does not require a structured mesh generation. Even for partial differential equations of high order, such as the one used in this paper, they do not suffer from the classical truncation error presented in the finite difference or finite volume methods. The use of a pseudo-random distribution of the collocation points showed good results. Thus, the RBF-MHD model can be used in complex geometries, where the grid generation is difficult. The RBF formulation, however, needs more research in order to specify the best shape parameter in less computing time.

Acknowledgements

This work was partially funded by CNPq, CAPES (agencies for the fostering of science from the Brazilian Ministry of Science and Education) and FAPERJ (agency for the fostering of science from the Rio de Janeiro State). The authors are also very thankful to Prof. Alain J. Kassab from University of Central Florida for his suggestions (during IPDO-2007 in Miami) on how to choose the best shape parameter for RBF approximations. The authors are also grateful for the partial financial support provided for this work by the US Air Force Office of Scientific Research under grant FA9550-06-1-0170 monitored by Dr. Todd E. Combs, Dr. Fariba Fahroo and Dr. Donald Hearn and by the US Army Research Office/Materials Division under the contract number W911NF-06-1-0328 monitored by Dr. William M. Mullins. The views and conclusions contained herein are those of the authors and should not be interpreted as necessarily representing the official policies or endorsements, either expressed or implied, of the US Air Force Office of Scientific Research, the US Army Research Office or the US. Government. The US. Government is authorized to reproduce and distribute reprints for government purposes notwithstanding any copyright notation thereon.

References

[1] E.J. Kansa, Multiquadrics – a scattered data approximation scheme with applications to computational fluid dynamics – II. Solutions to parabolic, hyperbolic and elliptic partial differential equations, Comput. Math. Appl. 19 (1990) 149–161.
[2] R.L. Hardy, Multiquadric equations of topography and other irregular surfaces, J. Geophys. Res. 176 (1971) 1905–1915.
[3] V.M.A. Leitão, A mesheless method for Kirchhoff plate bending problems, Int. J. Numer. Methods Eng. 52 (2001) 1107–1130.
[4] V.M.A. Leitão, RBF-based meshless methods for 2D elastostatic problems, Eng. Anal. Boundary Elem. 28 (2004) 1271–1281.
[5] H. Wendland, Error estimates for interpolation by compactly supported radial basis functions of minimal degree, J. Approx. Theory 93 (1998) 258–272.
[6] M.D. Buhmann, Radial Basis Functions: Theory and Implementations, Cambridge University Press, UK, 2003.
[7] G.S. Dulikravich, S.R. Lynn, Unified electro-magneto-fluid dynamics (EMFD): a survey of mathematical models, Int. J. Non-Linear Mech. 32 (5) (1997) 923–932.
[8] M.J. Colaço, G.S. Dulikravich, A multilevel hybrid optimization of magnetohydrodynamic problems in double-diffusive fluid flow, J. Phys. Chem. Solids 67 (2006) 1965–1972.
[9] J.P. Garandet, T. Alboussiere, R. Moreau, Buoyancy driven convection in a rectangular enclosure with a transverse magnetic field, Int. J. Heat Mass Transfer 35 (4) (1992) 741–748.
[10] N.M. Al-Najem, K.M. Khanafer, M.M. El-Refaee, Numerical study of laminar natural convection in tilted enclosure with transverse magnetic field, Int. J. Numer. Methods Heat Fluid Flow 8 (6) (1998) 651–672.
[11] J.P. Van Doormaal, G.D. Raithby, Enhancements of the SIMPLE method for predicting incompressible fluid flow, Numer. Heat Transfer 7 (1984) 147–163.
[12] G.D. Raithby, K.E. Torrance, Upstream-weighted differencing scheme and their application to elliptic problems involving fluid flow, Comput. Fluids 2 (1974) 191–206.
[13] B.P. Leonard, M.K. MacVean, A.P. Lock, The flux integral method for multidimensional convection and diffusion, Appl. Math. Modell. 19 (1995) 333–342.
[14] W.H. Press, B.P. Flannery, S.A. Teukolsky, W.T. Vetterling, Numerical Recipes FORTRAN, Cambridge University Press, 1992.
[15] E. Divo, A.J. Kassab, An efficient localized RBF meshless method for fluid flow and conjugate heat transfer, ASME J. Heat Transfer 129 (2) (2007) 124–136.
[16] S. Rippa, An algorithm for selecting a good value for the parameter c in radial basis function interpolation, Adv. Comp. Math. 11 (1999) 193–210.
[17] P.P. Chinchapatnam, Radial Basis Function Based Meshless Methods for Fluid Flow Problems, Ph.D. Thesis, Department of Mechanical Engineering, School of Engineering Sciences, University of Southampton, UK, 2006.
[18] M.M. El-Refaee, M.M. El-Sayed, N.M. Al-Najem, I.E. Megahid, Steady-state solutions of buoyancy-assisted internal flows using a fast false implicit transient scheme, Int. J. Numer. Methods Heat Fluid Flow 6 (6) (1996) 3–23.
[19] I. Sobol, Y.L. Levitan, The Production of Points Uniformly Distributed in a Multidimensional Cube, Institute of Applied Mathematics, USSR Academy of Sciences, vol. 40, 1976.